The diurnal cycle of water ice on comet 67P/Churyumov–Gerasimenko

M.C. De Sanctis[1]*, F. Capaccioni[1], M. Ciarniello[1], G.Filacchione[1], M. Formisano[1], S. Mottola[2], A. Raponi[1], F. Tosi[1], D. Bockelée-Morvan[3], S. Erard[3], C. Leyrat[3], B. Schmitt[4], E. Ammannito[5,1], G.Arnold[2], M.A. Barucci[3], M. Combi[6], M.T. Capria[1], P. Cerroni[1], W.-H. Ip[7], E. Kuehrt[2], T. B. McCord[8], E. Palomba[1], P. Beck[4], E. Quirico[4] and VIRTIS team.

[1] Istituto di Astrofisica e Planetologia Spaziali – INAF, via del fosso del cavaliere 100, 00133 Rome Italy.
[2] Institute for Planetary Research, DLR, Rutherfordstraße 2, 12489 Berlin, Germany.
[3] LESIA-Observatoire de Paris, CNRS, Universite´ Pierre et Marie Curie, Universite Paris Diderot, 5 place Jules Janssen, 92195 Meudon, France.
[4] Univ. Grenoble Alpes – CNRS Institut de Planetologie et Astrophysique de Grenoble Batiment D de Physique B.P. 53 38041 Grenoble Cedex 9 , France.
[5] University of California, Los Angeles, California 90095, USA. CA, USA.
[6] Department of Atmospheric, Oceanic and Space Sciences University of Michigan, 2455 Hayward Street, Ann Arbor, MI 48109, USA.
[7] National Central University, No. 300, Jhongda Rd., Jhongli District, Taoyuan City 32001, Taiwan Taipei, Taiwan.
[8] Bear Fight Institute, 22 Fiddler's Road, Box 667, Winthrop, Washington 98862, USA.

Observations of cometary nuclei have revealed a very limited amount of surface water ice[1–7], which is insufficient to explain the observed water outgassing. This was clearly demonstrated on comet 9P/Tempel 1, where the dust jets (driven by volatiles) were only partially correlated with the exposed ice regions[8]. The observations[6,7] of 67P/Churyumov–Gerasimenko have revealed that activity has a diurnal variation in intensity arising from changing insolation conditions. It was previously concluded that water vapour was generated in ice-rich subsurface layers with a transport mechanism linked to solar illumination[1–3,5], but that has not hitherto been observed. Periodic condensations of water vapour very close to, or on, the surface were suggested[3,9] to explain short-lived outbursts seen near sunrise on comet 9P/Tempel 1. Here we report observations of water ice on the surface of comet 67P/Churyumov–Gerasimenko, appearing and disappearing in a cyclic pattern that follows local illumination conditions, providing a source of localized activity. This water cycle appears to be an important process in the evolution of the comet, leading to cyclical modification of the relative abundance of water ice on its surface.

The Visible Infrared and Thermal Imaging Spectrometer VIRTIS[10] has collected high spatial (7-25 m/pixel) and spectral resolution data since Rosetta approached the comet nucleus in August 2014. The

reflectance spectra taken in different areas over the illuminated regions of the comet's nucleus, show a broad absorption band at 2.8-3.6 μm, attributed to organic compounds. The absence of pure water ice absorption band indicates an upper limit of about 1% (in volume) of the water ice , in very limited surface regions, at VIRTIS resolution[4].

Fig.1 shows a small region of the "Neck" (Lon 325°E ± 4°, Lat 31°N ± 5°, called "Hapi") of the comet, located between the small and large lobes of the nucleus, observed at different rotational phases after one or more comet rotations. During each rotation, this region moves into the shadows projected by the "Head" (the smaller lobe) bulge. VIRTIS observes variations in the absorption band near 3 μm as this region moves out of the shadow and becomes illuminated (Fig. 2a). In this case we observe a clear alteration of the organic compounds band, with a broadening, a shift towards shorter wavelengths and a strong increase in depth with decreasing illumination. The band center shifts from 3.18 ± 0.05-μm to 3.10±0.05-μm, its short-wavelength shoulder shifts from 2.82±0.05-μm to 2.71±0.05-μm, and the band depth relative to the continuum increases from 0.2±0.03 to 0.6±0.03. We also observe a flattening of the continuum slope and a reduced thermal emission as the 3-μm band depth increases.

The stronger 3-μm band, and the flattening of the continuum suggest exposed water ice, in addition to the organic material ubiquitously present on the comet surface[4] . The spectral ratio (Fig.2) shows the presence of a strong ice band extending from 2.7-μm to 3.6-μm, while the other water ice bands at 1.5 and 2.0-μm are not detected[11] (see Extended Data Fig.1) The 3-μm water band is clearly present in all the pixels located at the border of the shadowed region. The same region has been observed again one and four nucleus revolutions[12] later (Fig.1b,c,d) under slightly different illumination conditions, as shown by the shadows which cover different areas. Nevertheless, in each observation, the presence and change in the water absorption band depth is controlled by the shadow

location and not by the specific surface region. VIRTIS observes areas in which the spectra display progressive 3-µm band weakening as the region moves into greater illumination. Shadowed areas are slightly different in the VIRTIS observations (Fig.1b,c,d) and ice-rich and ice-free pixels change according to their distance from the shadow: ice-free pixels in the first observation (Fig.1b) show the ice signature (ice-rich) on the following observation (Fig.1c,d) where they are now closer to the shadow.

Using optical constants[13-16] and scattering theory[17] we modeled the spectra as an intimate mixture of ice and a dark non-ice component (SI, Extended Data Fig. 1, Extended Data Fig. 2) and derived water-ice abundance maps (Fig.3). The fit of the spectra requires a relative abundance up to of 10-15% water ice intimately mixed with the non-ice component, as shown in the ice distribution maps (Fig.3a). The maps indicate that the maximum quantity of ice is found very close to the shadows in all the observations, even if the pixels close to the shadows are at a different location on the comet surface.

The spectra also show differences at wavelengths longer than 3.6-µm, due to variations of the thermal emission as the region moves into lesser solar illumination, with a correlation of stronger 3-µm band with weaker thermal emission, thus with lower temperatures. The nucleus surface temperatures were retrieved from the long-wavelength portion (> 4.5µm) of the VIRTIS spectra[18]. The temperatures retrieved for the pixels near the shadows are at most 160 K with an uncertainty of ±10 K, while the temperature of the well illuminated areas are up to 210 K with an uncertainty of ±2 K (Fig. 3b). The pixels showing the strongest 3-µm absorption have temperatures in the range 160-180 K and a derived ice content varying in a range between 5 ±1 % and 14±3% (Fig. 3). The measured temperatures for these pixels are consistent with the presence of water ice in the nucleus outer layers. Water ice sublimation pressure[19] varies by three orders of magnitude from temperatures in the shadowed areas (< 1 nbar), to temperatures in the illuminated areas, where the activity occurs. A clear anti-correlation of

ice abundance with temperatures is seen (Fig.3c) in the regions near the shadows of Fig.1b, indicating that the temperature is cold enough to maintain ice at, or near, the surface in the shadows.

Most of the activity observed in the period of August-September 2014 is from the comet neck[6,7], where the region previously examined is located (Fig. 1a). Activity from this specific region is seen in all the data presented here, especially in the last acquired data (Fig. 1e)**,** indicating that a source for water exists to sustain the flux. The amount of water flux coming from the superficial ice documented by VIRTIS, represents ~ 3% of the total water flux measured by MIRO[6] (see Methods for calculations). We can extrapolate that a much larger area is affected by the same mechanism, although not directly observed, thus contributing to a larger amount to the total water flux. Indeed, all the Hapi region is subjected to this diurnal shadowing effects which can lead to the outgassing over much larger areas. It must be mentioned that the contribution to the total outgassing from these surface layers sources is limited in time. This is demonstrated by the progressive decrease of the abundance of deposited water ice in pixels exposed for a longer time to the solar illumination (see Fig.3).

In the case studied here, the presence of surface ice close to the location of the jets indicates that the outgassing source is likely in the uppermost layers of the surface.

The above description of the VIRTIS observations of ice sublimating in this neck's region when an area emerges from shadow and the progressive decrease of the ice abundance away from the shadow, clearly indicate that a cyclic sublimation–condensation process is at work during each comet rotation.

Two possible mechanisms for the cyclic condensation of water on unilluminated areas can be considered: 1) the condensation of water vapour present in the coma, and/or redeposition of icy grains, in cold areas on the nucleus[20,21], or 2) direct condensation of gas sublimating from the subsurface under appropriate thermodynamic conditions[9,22-24]. The first case could indeed occur in the region of the neck where, because of the large concavity, sublimated molecules from an illuminated region could impact

and condense on nearby non-illuminated areas. However, this mechanism seems to be more efficient at small heliocentric distance when gas production rate is high enough to enhance the re-deposited flux significantly[20].

The second mechanism has been already suggested to explain the outbursts observed by the Deep Impact mission on comet 9P/Tempel 1 that appear to occur near sunrise on a particular area[9], while extensive subsurface sources were invoked to explain the overall ambient outgassing as the observed area of exposed pure ice have a too limited extent[2]. In addition, during the fly-by of 103P/Hartley 2, the DIXI mission has revealed surface ice, notably only along the morning terminator, suggesting diurnal effects[25].

The VIRTIS observations are now able to demonstrate that a similar mechanism is at work; our nucleus thermo-physical model, along with previous literature[9,22,24], enables quantifying the diurnal cycle of water. When the surface is illuminated, water ice sublimates mainly from the uppermost surface layers (Fig. 4, Extended Data Fig. 3,4). When the surface goes into shadow (or into the night side), a temperature inversion occurs between the now colder surface layer and the interior layers which maintain a higher temperature for a longer time; the magnitude of this process is controlled by the duration of the shadow/night period and by the thermal inertia of the material and extends to a depth defined by the thermal skin depth. In the present case, the thermal inertia is constrained by independent measurements[4,6] and gives rise to a thermal skin depth of the order of few cm (Fig. 4 and Extended Data Fig. 4).

Thus, within the few cm affected by the heat exchange, water vapor still produced by subsurface sublimation in the warmer subsurface layers flows through the pores and could re-condense if the thermo-physical conditions of the colder upper surface layer allow re-condensation. By this mechanism the surface layer becomes enriched in water ice. The water ice in the uppermost surface layers will be

stable until a new cycle of solar illumination starts which will increase the surface temperature and thus will trigger again the comet water outgassing (Extended Data Fig. 3).

We thus suggest that the cyclic sublimation–condensation of ice triggered by varying illumination conditions, is a general process acting on cometary nuclei. This process implies the cyclical modification of the relative abundance of water ice on the surface of the comet, contributing to the local water activity. This mechanism could lead to differential erosion of the surface producing morphological differences or enhancing prior existing inhomogeneities. This mechanisms could also contribute to activity arising from the pits on comet 67P/Churyumov–Gerasimenko[26], being relevant the shadowing effects in the pits.

Moreover, the surface erosion could allow keeping the water ice close to the surface, thus avoiding fading of activity with time. Finally, as 67P/CG moves toward its perihelion, which will be reached in August 2015, the solar radiation increases with the inverse square of the heliocentric distance, and thus this process will become progressively more energetic, possibly leading to the formation of outbursts events like those observed on the nucleus of 9P/Tempel 1.

References and Notes:

1 Soderblom, L.A. *et al.,* Observations of Comet 19P/Borrelly by the Miniature Integrated Camera and Spectrometer Aboard Deep Space 1, *Science* **296**, 1087-1091 (2002).

2 Sunshine, J.M., *et al.,* Exposed Water Ice Deposits on the Surface of Comet 9P/Tempel 1 *Science* **311**, 1453- 1455 (2006).

3 A'Hearn, M.F., *et al.,* EPOXI at Comet Hartley 2, *Science* **332**, 1396-1400 (2011).

4 Capaccioni, F., *et al.,* The organic-rich surface of comet 67P/Churyumov-Gerasimenko as seen by VIRTIS/Rosetta, *Science,* **347**, doi:10.1126/science.aaa0628 (2015).

5 Feaga, L.M. *et al.,* Asymmetries in the distribution of H_2O and CO_2 in the inner coma of Comet 9P/Tempel 1 as observed by Deep Impact, *Icarus* **190**, 345- **356** (2007).

6 Gulkis S. *et al.,* Subsurface properties and early activity of comet 67P/Churyumov-Gerasimenko *, Science,* **347,** doi: 10.1126/science.aaa0709 (2015).

7 Sierk, H. *et al.*, On the nucleus structure and activity of comet 67P/Churyumov-Gerasimenko *Science,* **347,** doi 10.1126/science.aaa1044 (2015).

8 Farnham et al, Dust coma morphology in the Deep Impact images of Comet 9P/Tempel 1, *Icarus*, **191**, 146-160 (2007)

9 Prialnik, D. A'Hearn M. F. and Meech K. J., A mechanism for short-lived cometary outbursts at sunrise as observed by Deep Impact on 9P/Tempel 1, *Mon. Not. R. Astron. Soc.* **388***,* L20–L23 (2008)

10 Coradini, A. *et al.,* An Imaging Spectrometer for the Rosetta Mission, *Space Sci. Rev.* **128**, 529-559 (2007).

11 Filacchione, G., *et al.,* Saturn's icy satellites and rings investigated by Cassini-VIMS: III - Radial compositional variability, *Icarus,* **220**, 1064-1096 (2012).

12 Mottola, S., *et al.,* The rotation state of 67P/Churyumov-Gerasimenko from approach observations with the OSIRIS cameras on Rosetta, *Astron. and Astrophys.,* **569**, L2, doi:10.1051/0004-6361/201424590 (2014).

13 Warren, S.G, Optical constants of ice from the ultraviolet to the microwave*, Appl. Opt.,* **23**, 1206-1225 (1984).

14 Mastrapa R.M., *et al.* Optical constants of amorphous and crystalline H_2O-ice in the near infrared from 1.1 to 2.6 μm*, Icarus,* **197**, 307-320 (2008).

15 Mastrapa*,* R.M., *et al.,* Optical Constants of Amorphous and Crystalline H_2O-ice: 2.5-22 μm (4000-455 cm^{-1}) Optical Constants of H_2O-ice, *Astrophys. J.* , **701**, 1347-1356 (2009).

16 Clark, R.N. *et al.,* The surface composition of Iapetus: Mapping results from Cassini VIMS, *Icarus,* **218**, 831-860 (2012).

17 Hapke, B. Theory of reflectance and emittance spectroscopy. Cambridge University Press. (2012).

18 Tosi, F., *et al.,* Thermal measurements of dark and bright surface features on Vesta as derived from Dawn/VIR, *Icarus,* **240**, 36-57 (2014).

19 Fray, N., and Schmitt, B., Sublimation of ices of astrophysical interest: A bibliographic review *Planetary and Space Science*, **57**, 2053-2080 (2009).

20 Rubin, M., *et al.,* Mass Transport around Comets and its Impact on the Seasonal Differences in Water Production Rates, *Astrophysical Journal*, **788**, 168 (2014).

21 Crifo, J. F.; Loukianov, G. A.; Rodionov, A. V. and Zakharov, V. V., Navier-Stokes and direct Monte Carlo simulations of the circumnuclear coma II. Homogeneous, aspherical sources, *Icarus* **163**, 479- 503 (2003).

22 De Sanctis, M. C., Lasue, J., Capria, M. T., Seasonal Effects on Comet Nuclei Evolution: Activity, Internal Structure, and Dust Mantle Formation, *Astronomical Journal***, 140**, 1-13**,** (2010).

23 Rosenberg, E.D. and Prialnik, D. , The effect of internal inhomogeneity on the activity of comet nuclei - Application to Comet 67P/Churyumov-Gerasimenko, *Icarus,* **209**, 753-765, (2010).

24 De Sanctis, M. **C**., Lasue, J., Capria, M. T., Magni, G., Turrini, D., Coradini, A., Shape and obliquity effects on the thermal evolution of the Rosetta target 67P/Churyumov-Gerasimenko cometary nucleus, *Icarus*, **207**, 341-358, (2010)

25 Sunshine, J.M. *et al.,* Water Ice on Comet 103P/Hartley 2, EPSC-DPS Joint Meeting 2011, p.1345 (2011).

26 Vincent, J.B. et al, Large heterogeneities in comet 67P as revealed by active pits from sinkhole collapse , *Nature*, doi:10.1038/nature14564, (2015)

Acknowledgements:

The authors would like to thank the following institutions and agencies, which supported this work: Italian Space Agency (ASI - Italy), Centre National d'Etudes Spatiales (CNES- France), Deutsches Zentrum für Luft- und Raumfahrt (DLR-Germany), National Aeronautic and Space Administration (NASA-USA). VIRTIS was built by a consortium from Italy, France and Germany, under the scientific responsibility of the Istituto di Astrofisica e Planetologia Spaziali of INAF, I, which guides also the scientific operations. The VIRTIS instrument development for ESA has been funded and managed by ASI, with contributions from Observatoire de Meudon financed by CNES, F, and from DLR, D. The authors wish to thank the Rosetta Science Ground Segment and the Rosetta Mission Operations .The VIRTIS calibrated data will be available through the ESA's Planetary Science Archive (PSA) Web site.

Author Contributions: M.C.D.S., F.C. contributed in the data analysis and to write the manuscript. G.F. and F.C. provided calibrated VIRTIS data. A.R. and M.C. provided the spectral fit. M.C.D.S., M.T.C., M.F. and S.T provided the thermal modelling. F.T. retrieved the temperatures. All authors contributed to the discussion of the results and to write the paper.

Author information: Correspondence and requests for materials should be addressed to M.C.D.S. (mariacristina.desanctis@iaps.inaf.it)

Figure 1. Images of the ice-rich area. a) OPNAV context image of the region under study (red box); **b,c,d, and e)** VIRTIS image at 0.7-μm of the region in the red box of Fig. 1a. The data in Fig. 1b, 1c, and 1d has been acquired on Sept. 12, 13, and 14, 2014 respectively. The VIRTIS data in Fig. 1b and 1c are separated by ~12 hours, corresponding to ~1 comet rotation, while the data in Fig. 1c and 1d are separated by 37.3 hours, corresponding to ~3 comet rotations. The colored dots in Fig. 1b indicate

the zones from which the spectra in Fig. 2 are taken. Fig. 1e is the same of 1d, but stretched to see the jet (white arrows).

Figure 2. Spectra of the areas in Fig.1. a) Spectra from Fig.1b going from illuminated pixels to shadow. Black, red and cyan spots in Fig. 1b correspond to black, red and cyan spectra, respectively, taken at steps of 1 pixel. At wavelengths >3.5-3.7 μm, the spectra show smaller thermal emission for the pixels closer to the shadow line. The retrieved temperatures are 175±8K, 184±5K and 195±4K for the cyan, red and black spots, respectively. **b)** Spectral ratio of the cyan and black spectrum of Fig. 2a (solid-line) and a synthetic spectrum of water[11] (grains size of 10-μm,dashed-line). Instrument filters are indicated by gray bars.

Figure 3. Ice and Temperature maps. a) Ice maps: abundances in volume as shown by the scale bar. The black pixels are those in shadow or out of the nucleus. Isolated bright pixels are due to instrumental artifacts. b) Temperature images. White colors correspond to high temperatures while red-brown colors to low temperatures. **c**) **Scatter plot of ice abundance vs temperature.** The data points are extracted from Fig. 3a and refer to the region of the neck near the shadow. The error associated to the ice amount is 20%, ~3% for the temperatures above 170K and ~5% for temperatures below 170K.

Figure 4. Temperature and water vapor vs time. a**)** Simulated temperature at different depths from the nucleus surface to the interior, along one rotational period, for a small region of the neck near the shadows. b**)** Simulated water gas vs time along one rotational period. The simulation has been done using the "Rome" model[22,24] (Methods) and the parameters reported in Extended Data Table 2.The grey bars correspond to un-illuminated periods of time due the combination of comet rotation and shadows.

Methods

Data

VIRTIS observations were acquired on September 2014 when the Rosetta spacecraft was orbiting at a distance of about 27 km from comet 67P/Churyumov–Gerasimenko's surface resulting in a spatial resolution on the ground of about 7 m/pixel. During this period the instrument was observing the morning hemisphere with a solar phase of about 60-70 degrees. VIRTIS-M-IR data were acquired in scan mode with an integration time of 3 sec. The characteristics of the data here used are reported in Extended Data Table 1.

Spectral modeling

In order to model nucleus surface spectra a solution of the radiative transfer equation in a particulate medium must be applied. In this paper we adopt the Hapke model[17]. Our analysis is performed on normalized spectra in order to rule out the effect of surface roughness and minimize photometric issues. We model the icy regions of the comet, following the equation (2) approach, as formed by a two end-members regolith made of a "dark terrain" (DT) and water ice. The DT represents the average spectrum of the comet surface after photometric correction. Water ice is modeled as in [27], starting from optical constants which are obtained from[13-16] to cover the VIRTIS wavelength range.

We investigated two mixing modalities: areal and intimate. Areal mixtures are obtained from a linear combination of the reflectances of water ice and DT:

$$r_{eff} = f r_{H_2O} + (1 - f) r_{DT} \qquad (1)$$

where f is the relative amount of water ice and r_{eff} is the effective reflectance of the medium. Intimate mixture ("salt and pepper") is modeled as a linear combination of the two end-members single scattering albedoes (w) and is given by:

$$w_{eff} = fw_{H_2O} + (1-f)w_{DT} \qquad (2)$$

where the derived w_{eff} is used to compute the final reflectance. In both cases, along with the amount of water, also the grain diameter d is retrieved.

The modeling of the observed spectra is performed by a retrieval procedure that searches for the minimum of the reduced chi-square (χ^2_R), namely the best fit between the modeled (r^m) and the observed (r^o) reflectance:

$$\chi^2_R = \sum_{j=1}^{N} \left(\frac{r_j^o - r_j^m}{\sigma_j} \right)^2 \frac{1}{DOF} \qquad (3)$$

where j identifies each band (λ), N is the total number of bands, DOF are the degrees of freedom.

The observed spectra are corrected for spikes and instrumental artifacts. Among the residual sources of error, like straylight and signal from the coma, instrumental noise is the main contribution to the error of the measured reflectance (σ_j).

In Extended Data Fig. 1 we report, as an example, the result of a typical spectral fit for a pixel exhibiting a certain amount of ice obtained in the intimate and the areal case. It can be noted that intimate mixing provides the best match with measured spectra. The reason is that areal mixing increases the relative depth of 1.5-µm and 2-µm absorption bands with respect to the 3-µm feature, while they are very weak or absent across the dataset investigated in this work. Given this, the water ice abundance maps are obtained modeling the spectra as intimate mixtures.

The non-detection of the water ice bands at 1.5 and 2.0-μm indicates that the water ice and non-icy components are intimately mixed. In fact an areal mixture of 1% of water ice and 99% of non-ice materials yields spectra with well-defined absorptions features also at 1.5 and 2-μm as well as an increase in reflectance (Extended Data Fig. 1). This was the case of comet 9P/Tempel 1, where ice-rich patches on the nucleus have been modeled through an areal mixture containing 6±3% ice[2].

The maps showing the abundance of water ice (Fig. 3) are produced by setting a threshold of 50 on the median S/N of the spectra in order to avoid pixels in shadow or out of the nucleus of the comet.

In Extended Data Fig. 2, we report the spectra of three consecutive pixels going out of the shadow, and thus with decreasing abundance of water ice. The relative accuracy of the parameters obtained from the spectral modeling (water ice amount and grain diameter) is of the order of 20%, due to the instrumental noise and the uncertainty on the level of the dark terrain.

Estimation of water flux

The contribution to the total outgassing was estimated using only the extent of ice in our data. We calculated the surface area in the data that contains the transient ice and the percentage of ice in such an area. Using that information, with also the pixel size, we computed the equivalent area covered by pure ice. In the VIR data, this area is ~ 1 km^2.

MIRO measured about 10^{25} molec/sec and they estimated that between 0.1 and 1% of the 67P nucleus surface is needed to explain the water gas production rates if water ice were located on the surface[6]. Thus, using these values we can say that the "transient ice" seen by VIRTIS contributed ~ 3% to the total water flux. However, this this the lower limit of the contribution. In fact we can extrapolate that a similar fraction of the neck region, that is subject of a similar diurnal illumination effect, could have ice deposits as the imaged area.

Thermo-physical model

We applied a thermo-physical model [22,24, 29,30,] called the "Rome" model. We assume a porous, initially homogeneous nucleus composed of water ice and dust. Parameters used in these simulations are derived from the observations of 67P/Churyumov–Gerasimenko when available, or otherwise chosen among those that are considered typical for comets. The parameters used are detailed in Extended Data Table 2.

This model has been used in order to study the surface and subsurface temperature and the water flux emission of the "neck" region of the comet. The model can be applied to different comet regions, using as reference the shape model derived from the OSIRIS data, which covers the entire surface of the comet. We calculated the model for several facets but, here, for brevity, we focused on the facet number 14083 of the shape (V4), that is located in the neck region, where the phenomenon of sublimation–recondensation occurs. We computed the illumination over that facet, taking care, not only of the change in illumination due to the comet rotation around its axis, but also of the shadows created by the nearby facets. We followed the thermal evolution of the facet for several rotations, at the heliocentric distance of 3.38 AU, which is the distance of comet during the VIRTIS observations.

Code availability: The code used to generate the thermal models of comet 67P is a direct implementation of a published model[24,29,30]. The code used to generate the spectral fit is described in the method section. The code used to retrieve the nucleus temperatures of comet 67P is a direct implementation of a published method[18].

Reference

27 Ciarniello, M., *et al.,* Hapke modeling of Rhea surface properties through Cassini-VIMS spectra, *Icarus* **214**, 541-545 (2011).

28 JPL Small-Body Database Browser: 67P/Churyumov-Gerasimenko. NASA/Jet Propulsion Laboratory.

29 De Sanctis, M. C., Capria, M. T. and Coradini, A. Thermal evolution model of 67P/Churyumov-Gerasimenko, the new Rosetta target, *Astron. and Astrophys*., **444**, 605-614 (2005).

30 Capria, M.T., Coradini, A., De Sanctis, M.C. and Blecka, M.I. P/Wirtanen thermal evolution: effects due to the presence of an organic component in the refractory material", *Plant. Space. Sci*., **49**, 9, 907-918, (2001).

Extended Data Table 1.: VIRTIS observations characteristics

Extended Data Table 2. Main parameters used in the comet model

Extended Data Figure 1: Spectral fit. The two mixing modalities, intimate (a) and areal (b), are modeled for the same spectrum, identified by its position in the acquired image (sample and line) and its spacecraft event time (scet). The three missing parts of the spectra are related to the wavelength ranges covered by the junctions of the filters which produce significant artifacts. They are thus removed during the fitting procedure. The spectra are normalized with respect to λ_0 = 1.8-μm. For the areal mixture case, the modeled absorption band at 2-μm is significant, even with the small abundance (f_{H2O}) and grain diameter (d_{H2O}) we retrieved. This implies a worse fit as indicated by the larger χ^2 variable. The intimate mixture is thus a better model of the spectra.

Extended Data Figure 2: Spectral fits of comet nucleus spectra with different ice content. From the panel a to c: the depth of the absorption band at 3.2-μm significantly decreases and the band center slightly moves toward longer wavelengths. In both cases the spectra are well modeled with a decreasing amount of water ice (f_{H2O}) and a constant grain diameter (d_{H2O}) of the water ice. The three missing parts of the spectra are related to the wavelength ranges covered by the junctions of the filters which produce artifacts that we exclude from the fitting procedure. The spectra are normalized with respect to λ_0 = 1.8-μm.

Extended Data Figure 3. **Water diurnal cycle.** In the case reported here the sublimation of water vapour takes place in a deeper layer (see cartoon for a graphic explanation); the water vapour filters up to the surface layers (which are essentially dehydrated as during the day we do not see any spectral signature of ice) where, finding lower temperature conditions (as we are in the night or in shadow), condense and is trapped as ice. The subsequent illumination of the surface led to absolute loss of the

condensed water vapour. This, in fact, is an effective mechanism of transport of H_2O from deeper layer to the surface.

Extended data figure 4. Temperature and water vapor profiles. a) Temperature profiles and b) water gas pressure profiles from the nucleus surface to the interior at different time: blue curve is the profile when the area is illuminated; red curve is the profile obtained 6 minutes after the occurrence of the shadow, and purple curve is about 40 minutes after the occurrence of the shadow.

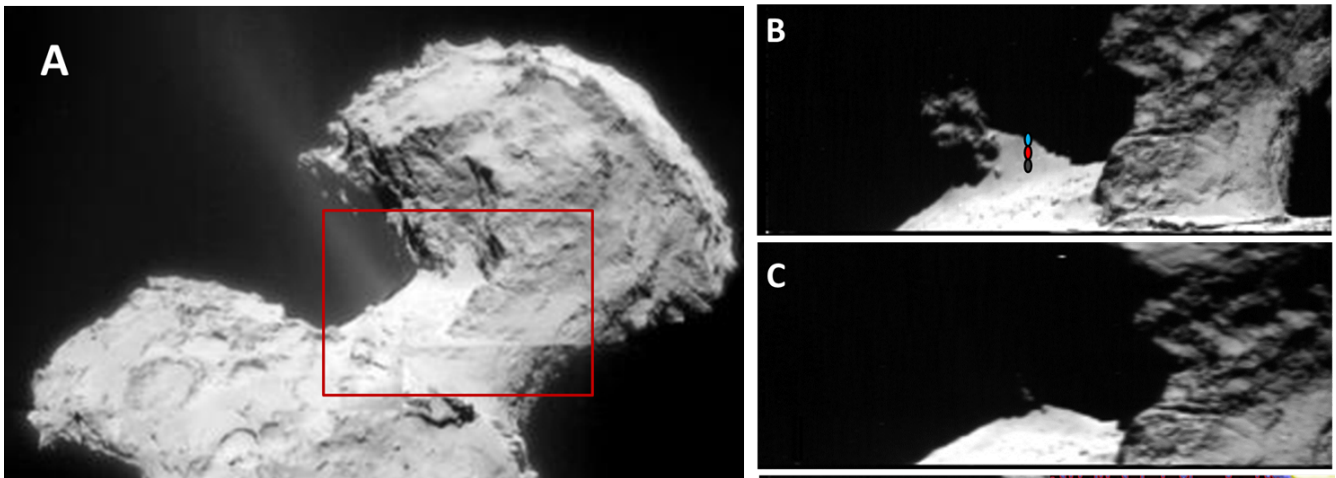

FIGURE. 1

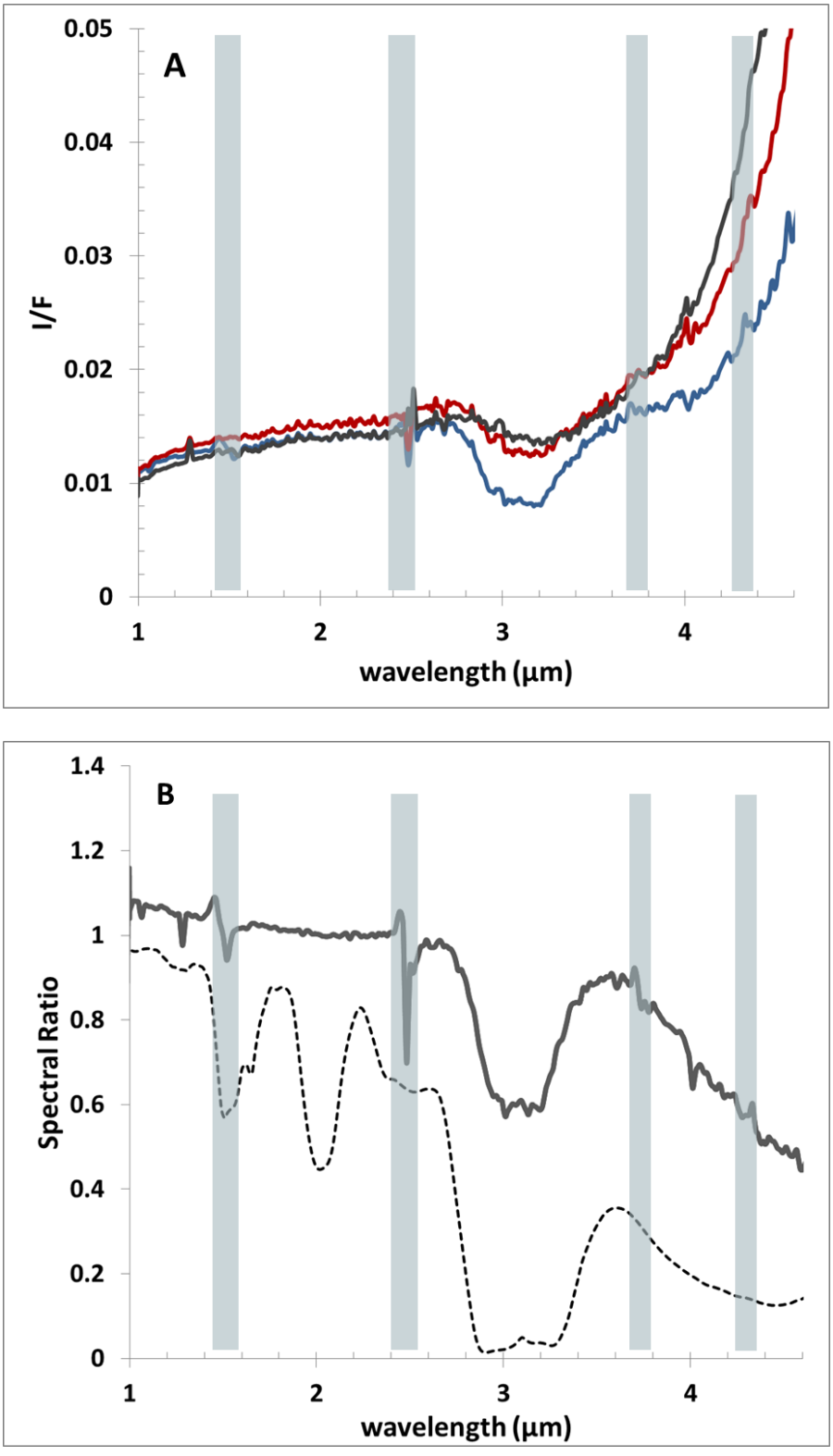
A
0.05
0.04
0.03
0.02
0.01
0
I/F
1
2
3
4
wavelength (µm)
B
1.4
1.2
1
0.8
0.6
0.4
0.2
0
Spectral Ratio
1
2
3
4
wavelength (µm)

Figure 2

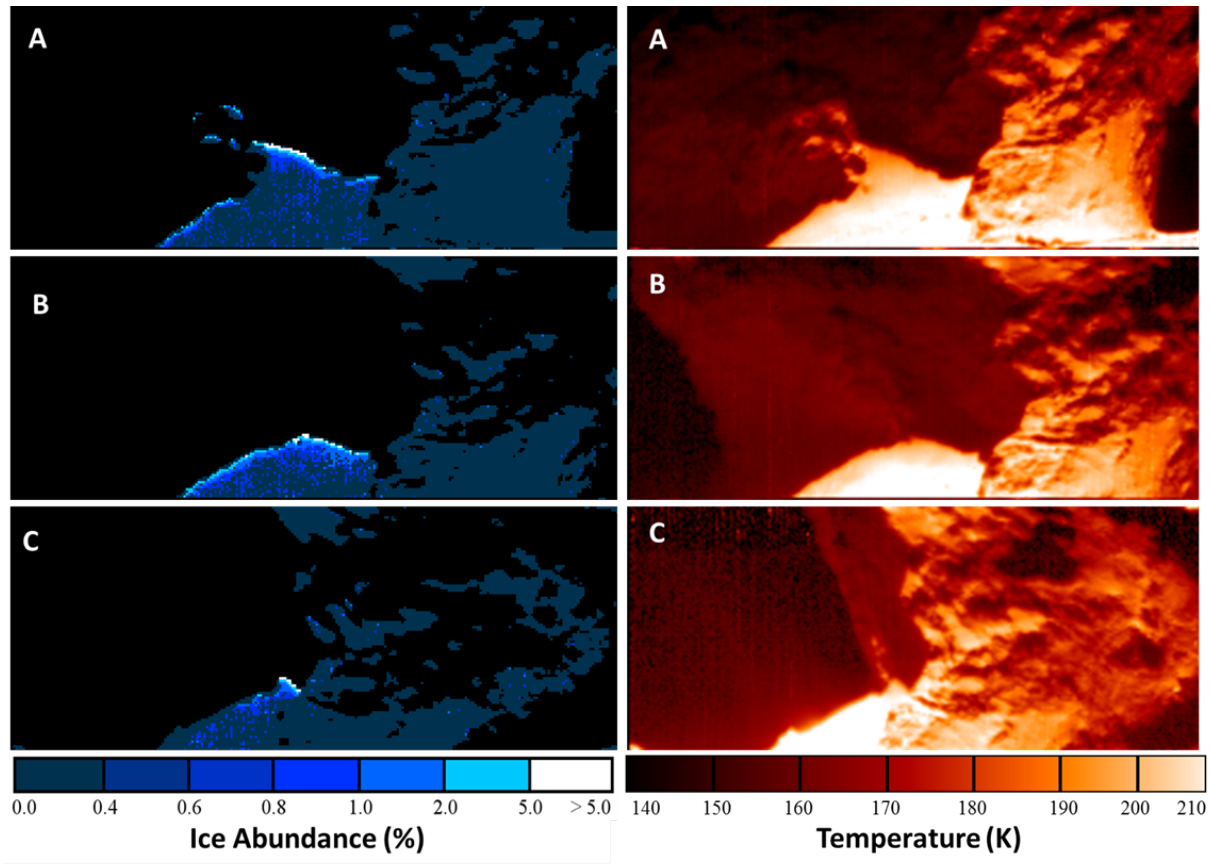
A
B
C
A
B
C
0.0
0.4
0.6
0.8
1.0
2.0
5.0
> 5.0
Ice Abundance (%)
140
150
160
170
180
190
200
210
Temperature (K)

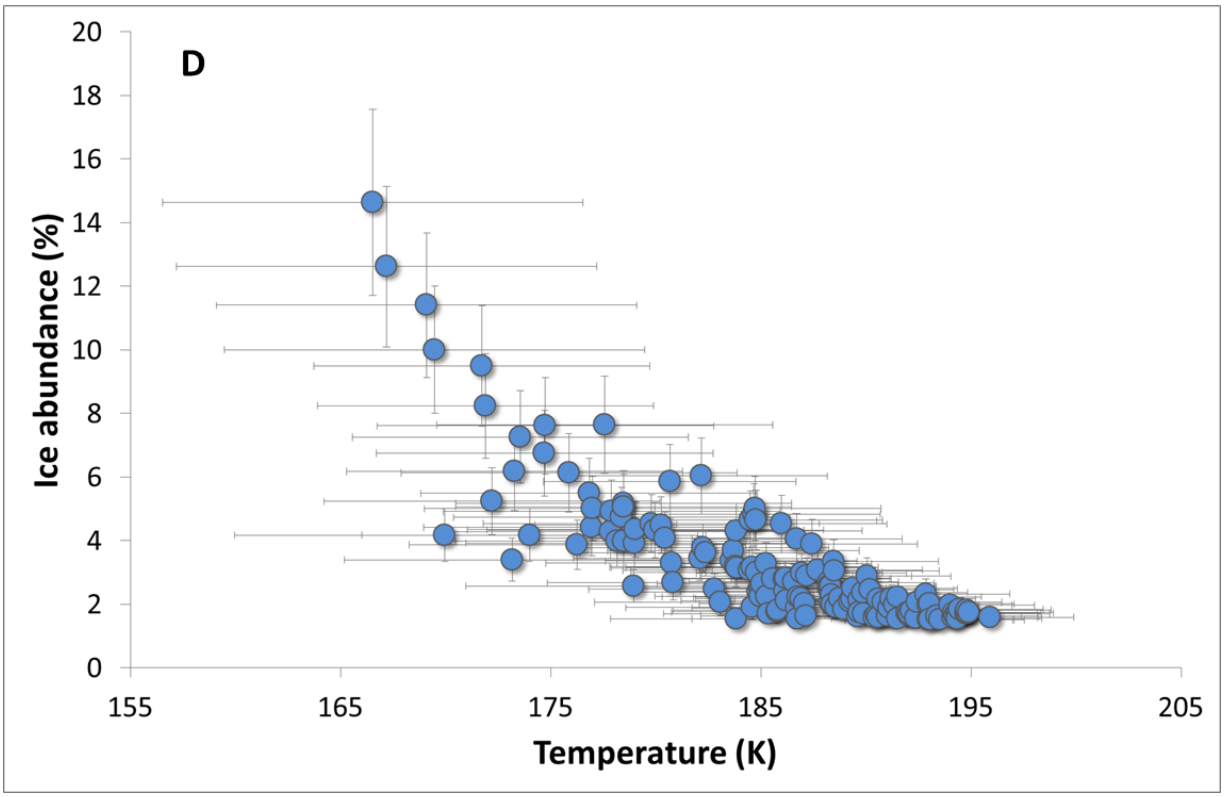
D
Ice abundance (%)
0
2
4
6
8
10
12
14
16
18
20
155
165
175
185
195
205
Temperature (K)

Figure 3

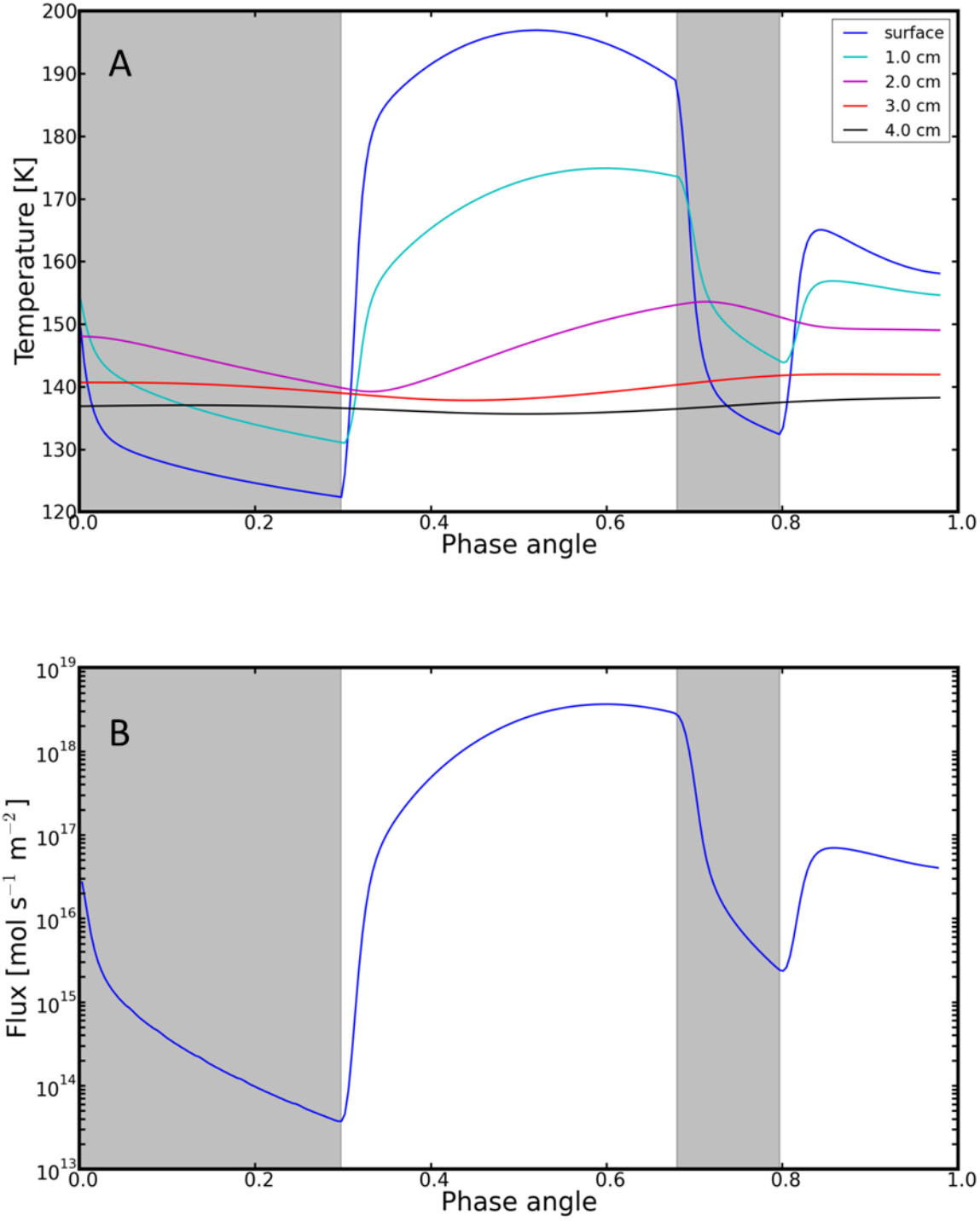
A
B
surface
1.0 cm
2.0 cm
3.0 cm
4.0 cm
Temperature [K]
Flux [mol s^{-1} m^{-2}]
Phase angle
Phase angle

Figure 4